AIP Journal of Applied Physics

Light collection optimization for composite photoanode in dye-sensitized solar cells: Towards higher efficiency

X. Z. Guo and W. Z. Shen

Citation: Journal of Applied Physics **117**, 225103 (2015); doi: 10.1063/1.4922413
View online: http://dx.doi.org/10.1063/1.4922413
View Table of Contents: http://scitation.aip.org/content/aip/journal/jap/117/22?ver=pdfcov
Published by the AIP Publishing

Light collection optimization for composite photoanode in dye-sensitized solar cells: Towards higher efficiency

X. Z. Guo[1] and W. Z. Shen[1,2,a)]
[1]*Institute of Solar Energy, Department of Physics and Astronomy, Shanghai Jiao Tong University, 800 Dong Chuan Road, Shanghai 200240, People's Republic of China*
[2]*Laboratory of Condensed Matter Spectroscopy and Opto-Electronic Physics, and Key Laboratory of Artificial Structures and Quantum Control (Ministry of Education), Department of Physics and Astronomy, Shanghai Jiao Tong University, 800 Dong Chuan Road, Shanghai 200240, People's Republic of China*

(Received 20 January 2015; accepted 29 May 2015; published online 11 June 2015)

Composite photoanode comprising nanoparticles and one-dimensional (1D) nanostructure is a promising alternative to conventional photoanode for dye-sensitized solar cells (DSCs). Besides fast electron transport channels, the 1D nanostructure also plays as light scattering centers. Here, we theoretically investigate the light scattering properties of capsule-shaped 1D nanostructure and their influence on the light collection of DSCs. It is found that the far-field light scattering of a single capsule depends on its volume, shape, and orientation: capsules with bigger equivalent spherical diameter, smaller aspect ratio, and horizontal orientation demonstrate stronger light scattering especially at large scattering angle. Using Monte Carlo approach, we simulated and optimized the light harvesting efficiency of the cell. Two multilayer composite photoanodes containing orderly or randomly oriented capsules are proposed. DSCs composed of these two photoanodes are promising for higher efficiencies because of their efficient light collection and superior electron collection. These results will provide practical guidance to the design and optimization of the photoanodes for DSCs. [http://dx.doi.org/10.1063/1.4922413]

I. INTRODUCTION

Since the breakthrough work achieved by O'Regan and Grätzel in 1991,[1] dye-sensitized solar cells (DSCs) have attracted substantial interest due to their low cost, high energy conversion efficiency, and eco-friendly production.[2–4] In conventional DSCs, a 10–20 μm thick film with a three-dimensional network of randomly dispersed, interconnected, spherical TiO_2 nanoparticles (NPs) 15–20 nm in diameter is employed as the photoanode. The mesoporous nanocrystalline film provides a large internal surface area for adsorbing dyes and ensures strong light absorption. In addition, the TiO_2 NP network also serves as an electron-transport media. When current is drawn from the cell, injected electrons transfer between TiO_2 NPs and move toward the anode contact. During their transport, electrons may be lost via recombination with the redox couples in electrolyte. The competition between electron transport and recombination determines the electron collection efficiencies (η_{col}).[5,6] Unfortunately, the electron transport in the TiO_2 NP network is slow due to the disordered geometrical structure and lattice mismatches at the grain boundaries.[7,8] Serious charge recombination and inefficient charge collection impede the further improvement of cell efficiency.

One strategy to overcome this problem is to fabricate the photoanode film from one-dimensional (1D) nanostructure TiO_2, such as nanorods (NRs),[9,10] nanowires (NWs),[11] nanotubes (NTs),[12] and nanofibers (NFs).[13] In particular, ordered 1D NT/NW arrays aligned vertically to the electron-collecting substrate have drawn extensive attention as an alternative to conventional TiO_2 NP network.[14–17] The ordered 1D nanostructure permits facile electron transfer along the long axis of the NT/NW, thereby minimizing the number of detrimental grain boundaries that one electron has to pass when traveling to the substrate.[18] Experimental measurements have shown that the electron recombination lifetimes and/or electron diffusion coefficients of 1D nanostructure were greater than those of NP-based films, indicating that the η_{col} was markedly enhanced.[19,20] However, the 1D nanostructure is not able to provide a high surface area for the anchoring of dye molecules, thus leading to insufficient light collection. The energy conversion efficiencies of 1D nanostructure-based DSCs reported to date are still far below those of NP-based ones.

The tradeoff between superior light collection and charge collection has became a bottleneck for DSCs. Attempts to circumvent this tradeoff involve the combination of high surface area NPs with highly conductive 1D nanostructure. Various designs have been tried: double- or multilayer films with NPs and NRs in separated layers,[21,22] NT arrays attached to a NP layer,[23] NT/NW arrays with NPs filling (deposing) the interstices,[24,25] *in situ*-growth of NW network within NP-based film,[26] and so on. Recently, Yen *et al.*[27] reported a composite photoanode by blending NTs with NPs. An optimized conversion efficiency of 10.27% has been achieved which is one of the highest reported efficiencies employing 1D nanostructure. Adachi *et al.*[28] fabricated photoanodes by mixing TiO_2 NWs of different concentrations with P-25 NPs and elucidated the necessity of highly crystallized 1D nanostructure for attainment of higher efficient DSCs. Similar composites made of NPs and 1D

[a)]Electronic mail: wzshen@sjtu.edu.cn.

nanostructure have also been reported by other researchers.[29–31] As a promising alternative to TiO_2 NP network, such composite photoanodes can maintain both a high surface area and efficient electron transport.

The 1D nanostructure mixed in the composite photoanodes is typically of submicron size with non-negligible light scattering effect in the visible region. Consequently, this 1D nanostructure will inevitably influence the light collection. Previous studies based on conventional photoanodes showed that the light scattering of spherical submicron particles has both positive and negative effects:[32,33] on one hand, the foreword light scattering can increase the optical path length of photons and thus enhance the light harvesting efficiency ($\eta_{\rm LHE}$) in red region; on the other hand, the light loss due to backward scattering may result in lower $\eta_{\rm LHE}$. Presumably, similar phenomena also exist in the composite photoanodes. That means the negative effect will deteriorate the light collection and thereby counteract the advantage on electron collection if the film structure is not designed properly. Up to now, little work has been done on the optimization of composite photoanode from the perspective of light collection. Poorer $\eta_{\rm LHE}$ is possibly a main obstruction to increase the cell efficiency using composite photoanodes.

In this paper, we theoretically investigated the light scattering properties of 1D nanostructure and their influence on the $\eta_{\rm LHE}$. The 1D nanoparticle mixed in the films is supposed to be capsule-shaped. Effects of capsule's size, shape, and orientation on the far-field scattering and the light harvesting are examined. Our goal is to optimize the film structure and propose a composite photonanode whose light collection performance is comparable to or better than that of conventional photoanode.

II. THEORETICAL MODEL

The photoanode films studied are composed of 20 nm spherical particles and submicron capsules. The capsules are uniformly dispersed with random or orderly orientation in each film layer. In our simulations, the total film thickness is fixed as 20 μm, and N719 dye is chosen as the sensitizer.

The far-field scattering intensity ($|E(\theta,\varphi)|^2$) for a single capsule is calculated by three-dimensional finite-difference time-domain (FDTD) method using a commercial software package (FDTD Solutions, Lumerical Solutions, Inc.). The θ and φ are azimuth angles as shown in Fig. 1. Apparently, the $|E(\theta,\varphi)|^2$ is dependent on the orientation of the capsule as well as its equivalent spherical diameter (D_e, diameter of a sphere having the same volume as the capsule) and aspect ratio (AR). The orientation of a capsule is described by ω which is the angle between the capsule's lengthwise orientation and the incident light direction (see Fig. 1).

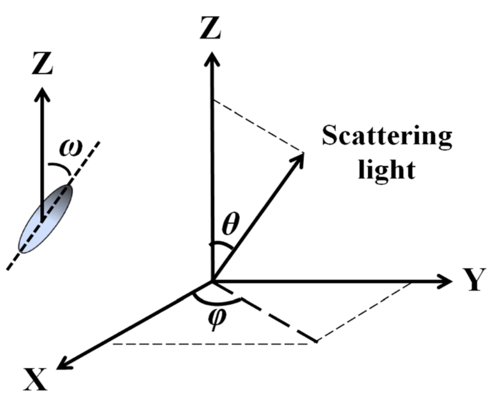

FIG. 1. Schematic diagram of scattering light's azimuth angles and capsule's orientation. The incident light propagates along the Z axis.

The η_{LHE} of composite photoanodes under considered is calculated by simulating the trajectory of 10^6 photons based on Monte Carlo method. Similar approaches have also been used for conventional photoanodes consisting of spherical scattering particles.[33–36] The trace simulation of a photon is carried out with the following steps. First, transmission length l, the distance traveled before experiencing either absorption or scattering, is calculated by the expression

$$l = -\ln[r]/(\alpha_{\rm abs} + \alpha_{\rm sca}), \tag{1}$$

where r is a random number comprised in the range $0 < r \le 1$, $\alpha_{\rm abs}$ and $\alpha_{\rm sca}$ are the light absorption and scattering coefficient, respectively. Second, absorption or scattering is determined by a second random number r'. If $r' \le \alpha_{\rm sca}/(\alpha_{\rm abs} + \alpha_{\rm sca})$, the photon is scattered, and the scattering angle is determined by a third random number r''. Then, the simulation returns to the first step. If $r' > \alpha_{\rm sca}/(\alpha_{\rm abs} + \alpha_{\rm sca})$, the photon is absorbed. The simulation is over when the incident photon is absorbed or goes out of the film. In our simulation, multiple light scattering of capsules is taken into account. Since the light scattering is dependent on capsule's orientation, the value of ω should be calculated and reset at each scattering step when the photoanode contains ordered capsules. In the case that capsules are randomly oriented, a new parameter, named equivalent far-field scattering intensity ($|E_e(\theta)|^2$), is calculated as

$$|E_e(\theta)|^2 = \frac{1}{2\pi}\int_0^{2\pi}\int_0^{\pi/2} |E(\theta,\varphi)|^2 \sin\omega d\omega d\varphi. \tag{2}$$

Thus, the orientation of capsules no longer needs to be considered in the calculation.

III. RESULTS AND DISCUSSION

A. Randomly oriented capsules

Figure 2 displays the $|E_e(\theta)|^2$ of randomly oriented capsules ($D_e = 150$ nm) at $\lambda = 700$ nm. The incident light intensity is 1 V^2/m^2. In the inset, the sum of $|E_e(\theta)|^2$ in all directions is normalized so that the changes in angular distribution can be seen more clearly. The $|E(\theta)|^2$ of a single spherical particle (AR = 1) is also drawn for comparison. As the capsule AR increases, the $|E_e(\theta)|^2$ decreases significantly in each direction and the proportion of scattered light at $\theta > 40°$ becomes smaller. Similar changes have also been found at other wavelengths (not shown). In addition, the total scattering intensity in all directions increases with the capsule D_e when the AR is constant (Fig. S1).[37] Studies based on conventional photoanodes have confirmed that scattering particles might "reflect" the incident photons out of the film resulting in light loss. This light loss is proportionate to the

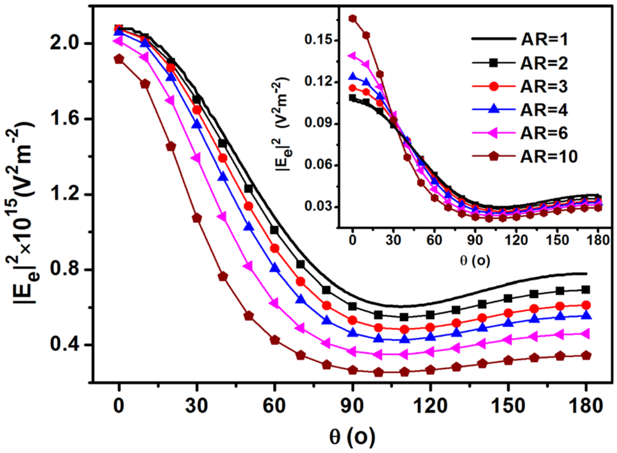

FIG. 2. Equivalent far-field scattering intensities ($|E_e(\theta)|^2$) of randomly oriented capsules ($D_e = 150$ nm) in nanocrystalline films calculated at $\lambda = 700$ nm. In the inset, the total scattering intensity in all directions is normalized.

film's light scattering coefficients α_{sca} at large angles. (The α_{sca} is the fraction of light scattered per unit distance in the film, and is determined by single particle's scattering intensity and particle concentration.) As shown in Fig. 2, the light scattering of single capsules is weaker than that of spherical particle especially at large angles. Consequently, it can be inferred that the light loss arising from back scattering would be effectively reduced by replacing the spherical scattering particles with randomly oriented capsules.

Figure 3 shows the calculated η_{LHE} of photoanodes with randomly oriented capsules of different AR. The capsules are embedded in the whole films uniformly with $D_e = 150$ nm and WF (weight fraction) = 20%. The black and red lines represent, respectively, the η_{LHE} of photoanodes without scattering particles (S0) and with spherical scattering particles (S-150) of the same D_e and WF. It can be seen that the η_{LHE} at $\lambda < 600$ nm decreases dramatically when mixing submicron particles, either spherical or capsule shaped, in the photoanode film. This decrease is entirely a consequence of light loss caused by back scattering. Consistent with our speculation, the η_{LHE} of photoanodes containing randomly oriented capsules is higher than that of S-150 in short wavelength region,

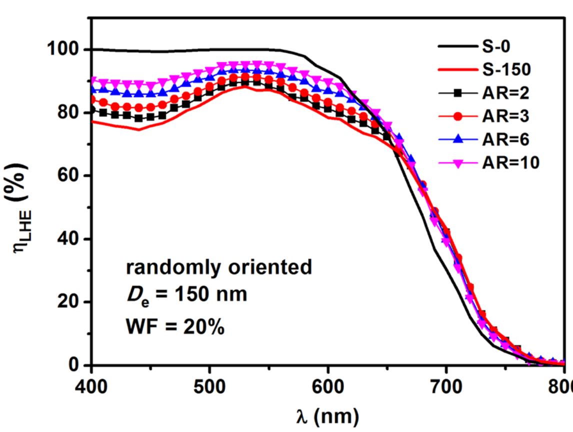

FIG. 3. η_{LHE} of photoanodes without scattering particles (S0), with spherical scattering particles (S-150), and with randomly oriented capsules of different AR.

and bigger AR corresponds to higher η_{LHE}. By analyzing the outgoing angles of photons at $\lambda = 500$ nm, it is found that the proportion of incident photons "reflect" out of the cell through the front surface decreases from 15.9% to 0.8% as capsule AR increases from 1 to 10. This result provides us direct evidence of the back scattering suppression.

Although the embedded submicron particles cause back scattering light loss, they increase the optical path lengths of incident photons and so their probability of being absorbed. Therefore, in the simulation model of Fig. 3, the η_{LHE} at $\lambda > 660$ nm is improved. Compared with S-150, the improvements of η_{LHE} in long wavelength region are slightly smaller when capsule AR > 1. This can be explained by the lower $|E_e(\theta)|^2$ of the randomly oriented capsules. We have also simulated photoanodes with capsules of different D_e, and similar changes in η_{LHE} were found (not shown).

B. Ordered capsules

The orientation of a capsule has an inevitable effect on its light scattering. Both the total intensity and angular distribution of scattered light change with the angle ω (Fig. S2).[37] Therefore, photoanodes with ordered capsules may present different light collection performances depending on the capsules' orientation. In this paper, we only discuss two representative cases, namely, the lengthwise orientation of capsules parallel or perpendicular to the incident light direction. For conciseness, these two orientations are referred to as vertical and horizontal, respectively.

Figure 4 depicts the distribution of far-field scattering intensities ($|E(\theta, \varphi)|^2$) for single capsules ($D_e = 150$ nm) at $\lambda = 700$ nm. The lengthwise orientation of each capsule is parallel to the incident light which propagates along the Z axis, so the $|E(\theta, \varphi)|^2$ is axially symmetric about this axis. Similar to the case of randomly oriented capsules, the $|E(\theta, \varphi)|^2$ of a vertical capsule decreases with the increase in AR. As a result, vertical capsules with larger AR tend to have

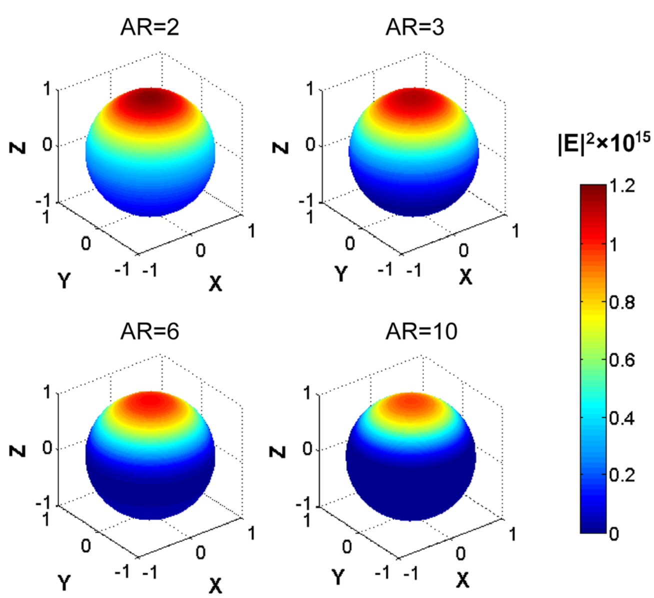

FIG. 4. Distribution of far-field scattering intensities ($|E(\theta, \varphi)|^2$) for single capsules ($D_e = 150$ nm) of different AR at $\lambda = 700$ nm. The incident light propagates along the Z axis, and $\omega = 0°$.

weaker back scattering and bring about higher η_{LHE} in short wavelength region (see Fig. 5). In the same simulation conditions (same D_e and WF), photoanodes with uniformly embedded vertical capsules show even better light collection than with randomly oriented ones at $\lambda < 650$ nm, indicating that vertical orientation is more capable of suppressing back scattering. When the capsule AR = 2 or 3, the η_{LHE} of photoanode is improved in the whole visible region compared with that of S-150. Further increase in AR leads to a decline of η_{LHE} at $\lambda > 650$ nm because of the shorter optical path length of incident photons. When the capsule AR is larger than 10, the $|E(\theta, \varphi)|^2$ is so small that the η_{LHE} curve almost overlaps with that of S0.

In the case that horizontal capsules uniformly embedded in the films, no improvement in η_{LHE} was found compared with photoanodes containing spherical scattering particles. Contrarily, the light collection performance becomes worse when the capsule $D_e > 200$ nm. Figure 6 displays the η_{LHE} of photoanodes with horizontal capsules ($D_e = 300$ nm, WR = 20%) of different AR. An obvious decrease in η_{LHE} can be found in the whole visible region as capsule AR increases from 2 to 6. As shown in Fig. 7, the $|E(\theta, \varphi)|^2$ distribution of a single horizontal capsule is non-axisymmetric. The light scattering on the directions, where $\varphi = 90°$ and $270°$, becomes relatively stronger and such a directionality property of light scattering is more noticeable for horizontal capsules with larger AR. In addition, the $|E(\theta, \varphi)|^2$ at $\theta > 90°$ increases with the capsule AR. These light scattering characteristics of horizontal capsules result in greater back scattering light loss and lower η_{LHE}.

C. Film structure optimization

The previous simulations are based on simple film structure, namely, single-layer photoanode with fixed parameters (D_e and WF) in the whole film. However, such a simple structure cannot achieve optimal light collection in a wide spectral range. Wang *et al*. have found that the light collection of DSCs depends strongly on the structure of photoanode film. They proposed a multilayer structure based on approximately-spherical scattering particles and obtained

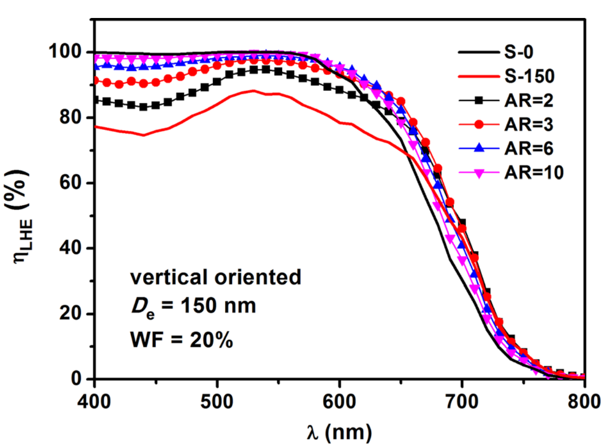

FIG. 5. η_{LHE} of photoanodes without scattering particles (S0), with spherical scattering particles (S-150), and with vertical capsules of different AR.

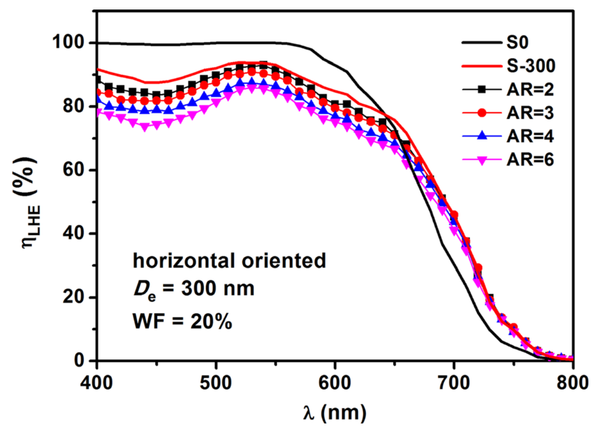

FIG. 6. η_{LHE} of photoanodes without scattering particles (S0), with spherical scattering particles (S-300), and with horizontal capsules of different AR.

significant improvements in cell performance.[32] Theoretical simulations have also proved that such a multilayer structure is superior to mono- and double-layer structures.[33] Here, we designed new multilayer structures by replacing the spherical scattering particles with capsules. In order to achieve the best light collection performance, we optimized the detailed structure of composite photoanodes, including the layer number, the thickness of each layer, and the D_e, AR, WF, and orientation of capsules in each layer.

The design guidance of multilayer photoanodes is to make the light scattering coefficient α_{sca} gradually increasing with the depth in the film. Thus, no or little incident light will be lost attributed to the weak scattering near substrate, and the long-wave absorption can be improved by the strong scattering in deeper layers. We carried out the structure optimization for two cases: in one case, the capsules are ordered in each layer; in the other case, the capsules are randomly oriented. Figure 8 demonstrates the optimal multilayer structures for each case. The M_capsule_1 in Fig. 8(a) consists of five layers. Both the D_e and WF increase gradually from the layer closest to the substrate. In the lower three layers, vertical capsules are employed, and the capsule AR is larger in the layer closer to the substrate. Such a design can efficiently suppress the back scattering light loss according to the results above. Horizontal capsules are used in the upper two layers. With larger back scattering intensities, these horizontal capsules can confine the incident light within the photoanode film. In M_capsule_2 [Fig. 8(b)], there are no scattering particles in the lowest layer to avoid the back scattering light loss, which is similar to Wang's multilayer structure. The capsule WF in the upper four layers is fixed as 30%. Such a high concentration of 1D nanoparticle is conducive to electron transport. The light scattering intensity in each layer is adjusted by capsule D_e and AR.

Figure 9 depicts the calculated η_{LHE} of M_capsule_1 and M_capsule_2. For comparison, we have also simulated conventional multilayer photoanodes containing spherical scattering particles. The best result, M_sphere, is also drawn in Fig. 9, and its detailed structure is given in Table I. It can be seen that $\eta_{LHE,\ M\_capsule\_1} \approx \eta_{LHE,\ M\_sphere} > \eta_{LHE,\ M\_capsule\_2} > \eta_{LHE,\ S0}$. The η_{LHE} at $\lambda > 550$ nm is dramatically improved, while the η_{LHE} at shorter wavelengths maintains $\sim$100%. The integral

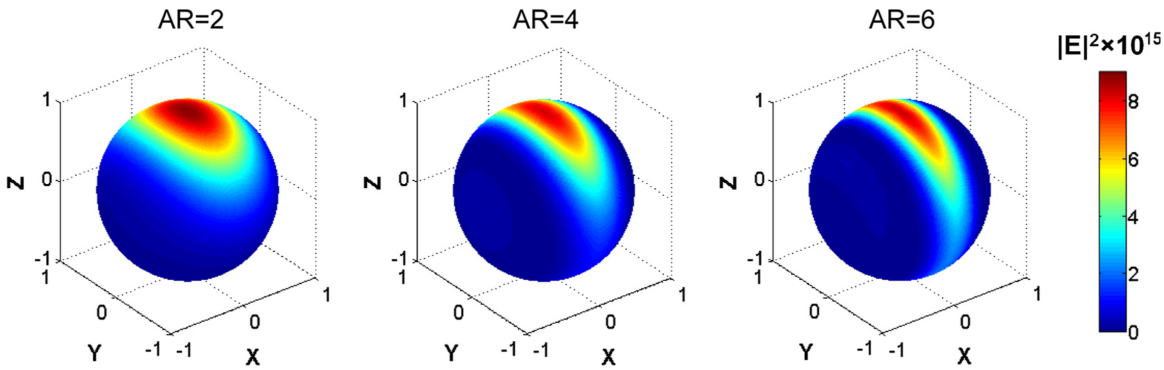

FIG. 7. Distribution of far-field scattering intensities ($|E(\theta, \varphi)|^2$) for single capsules ($D_e = 300$ nm) of different AR at $\lambda = 700$ nm. The lengthwise orientation of capsules is parallel to the X axis, and the incident light propagates along the Z axis.

results of η_{LHE} show that the overall difference of the three multilayer photoanodes in light collection is less than 1%.

In general, efficient light collection, electron injection, and charge transport are the three key factors indispensable to a high-performance photoanode. Since the electron injection process in TiO_2/Ru-bipyridyl dye films is ultrafast, orders of magnitude faster than the competing process of excited state decay to ground, the electron injection efficiency is almost 100%.[38] Then, the performance of a photoanode mainly depends on the other two factors. With standard diffusion model and linear recombination assumption, the steady-state solution for electron collection efficiency η_{col} at short-circuit condition can be written as[35]

$$\eta_{col}(\lambda) = \frac{1}{\cosh\left(\frac{d}{L}\right)} \times \frac{\int_0^d g(x,\lambda)\cosh\left[\frac{d-x}{L}\right]dx}{\int_0^d g(x,\lambda)dx}, \quad (3)$$

where d is the photoelectrode film thickness, g is the local electron generation rate, and L is the electron diffusion length. The η_{LHE} and g of the three multilayer photoanodes are similar, while the L of M_capsule_1 and M_capsule_2 are longer attributed to the capsules mixed in the films. DSCs composed of the two composite photoanodes would have higher η_{col} and thus higher energy conversion efficiency. A longer L also

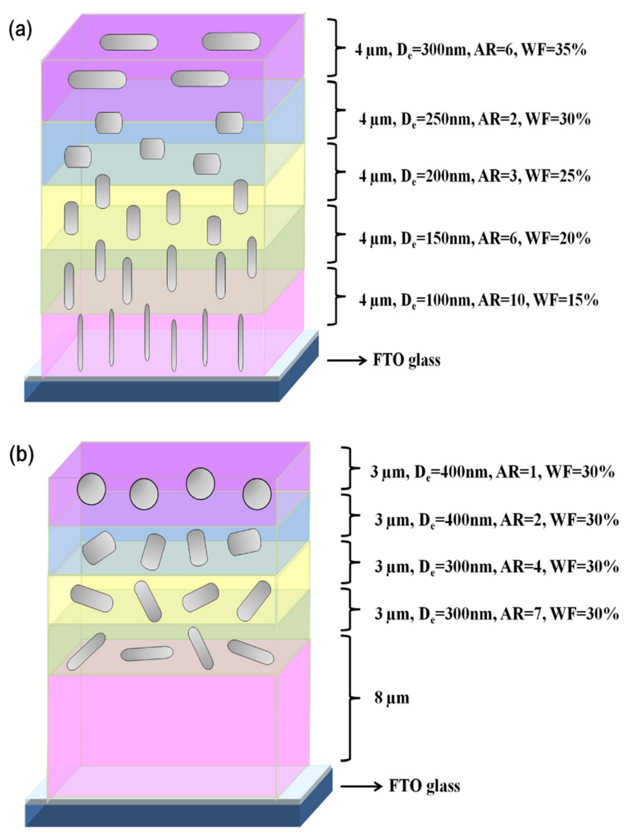

FIG. 8. Schematic film structures of optimal multilayer photoelectrodes: (a) M_capsule_1 and (b) M_capsule_2.

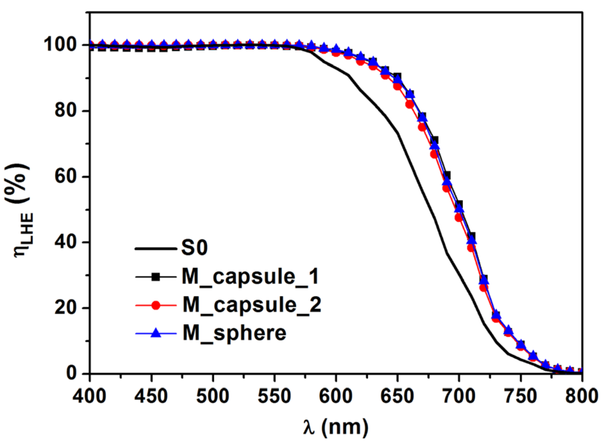

FIG. 9. η_{LHE} of optimal multilayer photoanodes without scattering particles (S0), with ordered capsules (M_capsule_1), randomly oriented capsules (M_capsule_2), and spherical scattering particles (M_sphere).

TABLE I. The detailed structure of multilayer photoanode M_sphere.

Sample	Layers[a]	Thickness (μm)	D[b] (nm)	WF[c] (%)
M_sphere	1	5	…	…
	2	3	200	10
	3	3	250	15
	4	3	300	20
	5	3	350	25
	6	3	400	30

[a]Layers are arranged according to the sequence beginning from the conducting substrate.
[b]D is the diameter of scattering particles.
[c]WF is the weight fraction of scattering particles.

means that the composite photoanodes can be thicker than the conventional ones without increasing the charge recombination. The traditional preparation methods (screen printing and doctor blade) are applicable to composite photoanodes containing randomly oriented capsules, so it is entirely feasible to further improve DSC's efficiency using photoanodes similar to M_capsule_2. Although there are no experimental reports on composite photoanodes with ordered capsules, this type of photoanode demonstrates better light collection performance according to our simulations. Moreover, vertical capsules are more conducive to electron transport. Consequently, such type of composite photoanode should be encouraged to fabricate in experiment. It should be pointed out that diffuse scattering designs of simple spherical particles in DSC already give rise to large boosts of efficiency, more sophisticated designs like the composite photoanodes herein proposed would only help to enhance it a little bit more.

IV. CONCLUSIONS

In summary, we theoretically investigated the light collection of composite photoanodes comprising small NPs and submicron capsules. The simulations indicate that capsules with bigger D_e or smaller AR demonstrate stronger light scattering. The large angle scattering intensity increases when the capsule's orientation changes from vertical to horizontal. Since the light scattering of capsules has both positive and negative impacts, the film structure should be carefully designed for attainment of optimal light collection. Based on the concept of multilayer structure, we proposed two composite photoanodes whose light collection performance is comparable to that of conventional photoanodes. DSCs composed of these two composite photoanodes are promising for higher efficiencies by taking advantage of the superior electron transport. It is believed that this work will provide practical guidance to the design and optimization of photoanodes employing 1D nanostructure, and will encourage the fabrication and application of DSCs with this kind of photoanodes. In the future, a more comprehensive model, combining the optical and electrical analysis,[39,40] is needed to give a more precise description on such composite photoanodes.

ACKNOWLEDGMENTS

This work was supported by National Major Basic Research Project (2012CB934302), Natural Science Foundation of China (11174202, 11204176, 61234005, and 11474201), China Postdoctoral Science Foundation (2012M520889), and Postdoctoral Research Program of Shanghai (13R21413500).

[1]B. O'Regan and M. Grätzel, Nature **353**, 737 (1991).
[2]M. Grätzel, J. Photochem. Photobiol., A **164**, 3 (2004).
[3]A. J. Frank, N. Kopidakis, and J. van de Lagemaat, Coord. Chem. Rev. **248**, 1165 (2004).
[4]A. Hagfeldt, G. Boschloo, L. Sun, L. Kloo, and H. Pettersson, Chem. Rev. **110**, 6595 (2010).
[5]G. Schlichthörl, N. G. Park, and A. J. Frank, J. Phys. Chem. B **103**, 782 (1999).
[6]H. K. Dunn and L. M. Peter, J. Phys. Chem. C **113**, 4726 (2009).
[7]N. Kopidakis, E. A. Schiff, N. G. Park, J. van de Lagemaat, and A. J. Frank, J. Phys. Chem. B **104**, 3930 (2000).
[8]L. Forro, O. Chauvet, D. Emin, L. Zuppiroli, H. Berger, and F. Levy, J. Appl. Phys. **75**, 633 (1994).
[9]S. H. Kang, S. Choi, M. Kang, J. Kim, H. Kim, T. Hyeon, and Y. Sung, Adv. Mater. **20**, 54 (2008).
[10]P. Kuo, T. Jan, C. Liao, C. Chen, and K. Lee, J. Power Sources **235**, 297 (2013).
[11]L. Wang, Z. Xue, X. Liu, and B. Liu, RSC Adv. **2**, 7656 (2012).
[12]X. Wang, G. He, H. Fong, and Z. Zhu, J. Phys. Chem. C **117**, 1641 (2013).
[13]E. Ghadiri, N. Taghavinia, S. M. Zakeeruddin, M. Grätzel, and J. Moser, Nano Lett. **10**, 1632 (2010).
[14]X. Feng, K. Shankar, O. K. Varghese, M. Paulose, T. J. Latempa, and C. A. Grimes, Nano Lett. **8**, 3781 (2008).
[15]D. Kim, A. Ghicov, S. P. Albu, and P. Schmuki, J. Am. Chem. Soc. **130**, 16454 (2008).
[16]B. Lei, J. Liao, R. Zhang, J. Wang, C. Su, and D. Kuang, J. Phys. Chem. C **114**, 15228 (2010).
[17]M. Yu, Y. Long, B. Sun, and Z. Fan, Nanoscale **4**, 2783 (2012).
[18]J. Villanueva-Cab, S. Jang, A. F. Halverson, K. Zhu, and A. J. Frank, Nano Lett. **14**, 2305 (2014).
[19]X. Feng, K. Zhu, A. J. Frank, C. A. Grimes, and T. E. Mallouk, Angew. Chem. Int. Ed. **51**, 2727 (2012).
[20]J. R. Jennings, A. Ghicov, L. M. Peter, P. Schmuki, and A. B. Walker, J. Am. Chem. Soc. **130**, 13364 (2008).
[21]R. Gao, Z. Liang, J. Tian, Q. Zhang, L. Wang, and G. Cao, RSC Adv. **3**, 18537 (2013).
[22]H. Wu, C. Lan, J. Hu, W. Huang, J. Shiu, Z. Lan, C. Tsai, C. Su, and E. W. Diau, J. Phys. Chem. Lett. **4**, 1570 (2013).
[23]X. Xin, J. Wang, W. Han, M. Ye, and Z. Lin, Nanoscale **4**, 964 (2012).
[24]M. Ye, X. Xin, C. Lin, and Z. Lin, Nano Lett. **11**, 3214 (2011).
[25]Z. Yang, D. Pan, C. Xi, J. Li, J. Shi, F. Xu, and Z. Ma, J. Power Sources **236**, 10 (2013).
[26]Y. Bai, H. Yu, Z. Li, R. Amal, G. Q. Max Lu, and L. Wang, Adv. Mater. **24**, 5850 (2012).
[27]Y. Yen, W. Ko, J. Chen, and K. Lin, Electrochim. Acta **105**, 142 (2013).
[28]M. Adachi, R. Tanino, J. Adachi, Y. Mori, K. Tsuchiya, S. Isoda, and F. Uchida, J. Power Sources **226**, 94 (2013).
[29]P. Joshi, L. Zhang, D. Davoux, Z. Zhu, D. Galipeau, H. Fong, and Q. Qiao, Energy Environ. Sci. **3**, 1507 (2010).
[30]K. Fan, W. Zhang, T. Peng, J. Chen, and F. Yang, J. Phys. Chem. C **115**, 17213 (2011).
[31]Q. Hu, C. Wu, L. Cao, B. Chi, J. Pu, and L. Jian, J. Power Sources **226**, 8 (2013).
[32]Z. Wang, H. Kawauchi, T. Kashima, and H. Arakawa, Coord. Chem. Rev. **248**, 1381 (2004).
[33]X. Z. Guo and W. Z. Shen, J. Appl. Phys. **114**, 074310 (2013).
[34]A. Usami, Sol. Energy Mater. Sol. Cells **64**, 73 (2000).
[35]F. E. Gálvez, E. Kemppainen, H. Míguez, and J. Halme, J. Phys. Chem. C **116**, 11426 (2012).
[36]F. E. Gálvez, P. R. F. Barnes, J. Halme, and H. Míguez, Energy Environ. Sci. **7**, 689 (2014).
[37]See supplementary material at http://dx.doi.org/10.1063/1.4922413 for the dependence of far-field scattering intensity on capsule D_e and orientation, respectively.
[38]N. A. Anderson and T. Lian, Annu. Rev. Phys. Chem. **56**, 491 (2005).
[39]A. B. Walker, L. M. Peter, M. J. Cass, P. J. Cameronb, and D. Martíneza, J. Mater. Chem. **15**, 2253 (2005).
[40]K. D. Benkstein, N. Kopidakis, J. van de Lagemaat, and A. J. Frank, J. Phys. Chem. B **107**, 7759 (2003).